Int. J. Electrochem. Sci., 11 **(2016)** 10199 – 10209, doi: 10.20964/2016.12.58

International Journal of
ELECTROCHEMICAL
SCIENCE
www.electrochemsci.org

Sn Embedded $Li_4Ti_5O_{12}$/C Composite as a High Capacity Anode Material for Li-ion Battery

Tianbiao Zeng, Xuebu Hu[*], *Penghui Ji, Qimeng Peng, Biao Shang*

College of Chemistry and Chemical Engineering, Chongqing University of Technology, Chongqing 400054, China
[*]E-mail: xuebu8006@126.com

Received: 4 September 2016 / *Accepted:* 29 September 2016 / *Published:* 10 November 2016

Sn embedded $Li_4Ti_5O_{12}$/C composite (C-Sn/$Li_4Ti_5O_{12}$) was prepared using TiO_2 sphere as precursor. The physical characteristics of C-Sn/$Li_4Ti_5O_{12}$ were characterized by X-ray diffraction (XRD), thermogravimetric analysis (TG), Raman spectra, elemental analysis, scanning election microscopy (SEM) and transmission electron microscopy (TEM). The electrochemical performances were investigated by cyclic voltamnograms (CVs) and galvanostatic charge-discharge tests. These analyses indicate that C-Sn/$Li_4Ti_5O_{12}$ was spherical-like particles about 1μm. Moreover, it was composed of inner spinel $Li_4Ti_5O_{12}$, outer-coated carbon layer and Sn embedded between inner $Li_4Ti_5O_{12}$ and outer carbon layer. Combining high specific capacity of Sn particles and high electronic conductive of carbon coated layer, as-prepared C-Sn/$Li_4Ti_5O_{12}$ shows improved discharge capacity. Compared with carbon-coated $Li_4Ti_5O_{12}$ (C-$Li_4Ti_5O_{12}$), the C-Sn/$Li_4Ti_5O_{12}$ exhibited better capability at 200 mA g^{-1} with a discharge capacity increased by ~ 16.3%. After 100 cycles, the discharge capacity of C-Sn/$Li_4Ti_5O_{12}$ was stable at ~ 242 mAh g^{-1}.

Keywords: $Li_4Ti_5O_{12}$; Sn; carbon layer; anode

1. INTRODUCTION

Exploring anode materials with high specific capacity and long cycle life for large-scale applications such as hybrid electric vehicles (HEV) and plug-in HEV is still main challenge for developing Li-ion batteries [1]. Due to high structure stability and safety, spinel $Li_4Ti_5O_{12}$ is considered as an alternative anode material [2-4]. Compared with commercial graphite of 372 mAh g^{-1} [5,6], the practical applications of $Li_4Ti_5O_{12}$ have been prohibited owing to its specific capacity is low as 175 mAh g^{-1} between 1V and 3V. In order to increase its capacity, one method is extending a charge-discharge voltage window from 1 - 3V to 0 -3V. Nugroho et al. prepared $Li_4Ti_5O_{12}$ powder in

supercritical water and cycled from 0V to 3V. The sample delivered an initial capacity of 212 mAh g^{-1} and retained ~ 200 mAh g^{-1} after 50 cycles at 1C [7]. Yi et al. synthesized $Li_4Ti_5O_{12}$ using a solid-state method and the sample exhibited a stable capacity of ~ 210 mAh g^{-1} after 150 cycles when it cycled from 0V to 2.5V at 1C [8]. Yu et al. obtained amorphous $Li_4Ti_5O_{12}$ thin film via a sol-gel method. As-prepared thin films showed a high initial capacity of 283.5 mAh g^{-1} and the capacity loss was only 3% after 100 cycles, but the cycle current was only 10 μA cm^{-2} [9]. Though the discharge capacity has been improved, there is a gap compared to graphite. Another strategy to increase the capacity of $Li_4Ti_5O_{12}$-based anode is doping by high capacity materials, such as SnO_2 [10-12] and Sn [13,14]. Compared to SnO_2, Sn has attracted wide attention due to its higher specific capacity (991 mAh g^{-1}). However, an obvious disadvantage of Sn is its large volume change (up to 360%) during the charge-discharge process, which will causes electrode serious pulverization and the decrease of electrical contact subsequently, even leading to rapid capacity degradation [15-18]. Li et al. synthesized Sn/C nanofibers with ~ 10 wt% Sn deposed on surface showed a discharge capacity of about 400 mAh g^{-1} after 20 cycles under 50 mA g^{-1} [19]. Cui et al. prepared core/shell-structured Sn@C maintained a high discharge capacity of 585mAh g^{-1} after 100 cycles at 0.1 A g^{-1} and delivered a high reversible capacity of 480 mAh g^{-1} at 5 A g^{-1} [20]. These references prove that carbon coating can improve the electrochemical performances of Sn anode. Here, coated carbon plays two different roles during cycling, leading to better capacity retention. One acts as a buffer layer that absorbs the internal stress causing by Sn expansion-contraction during cells cycling. The other is forming a conductive net between Sn particles, which improves the electronic conductivity of electrodes.

Herein, we demonstrate a synthesis route to spherical-like C-Sn/$Li_4Ti_5O_{12}$ particles with average outer diameter of ~1μm. Combining high specific capacity of Sn particles and high electronic conductive of carbon coated layer, it is desirable that as-prepared C-Sn/$Li_4Ti_5O_{12}$ shows improved discharge capacity and good cycle performance.

2. EXPERIMENTAL

2.1 Sample preparation

The TiO_2 spheres were firstly prepared by a reported sol-gel method with minor modifications [21]. In a typical synthesis, 80 mg heptanoic acid, 265 mg tetrabutyl titanate and 30 mL absolute ethanol were mixed and stirred, and then 2.25 mL deinonized water was added and stirred to form a white gel. Subsequently, the gel was put into a 100 mL Teflon-lined stainless autoclave and heated at 150℃ for 12h. After being isolated using centrifugation, washed with deinonized water and ethanol several times, the prepared TiO_2 spheres were dry in vacuum oven. For synthesizing $Li_4Ti_5O_{12}$, the as-prepared TiO_2 was ball milling with Li_2CO_3 in 5% lithium atom exceed using ethanol as dispersing agent, then the precursor was calcined at 800℃ in air for 20h to obtained $Li_4Ti_5O_{12}$ with temperature increased from room temperature in a rate of 5 ℃ min^{-1}. For C-Sn/$Li_4Ti_5O_{12}$, 232 mg $SnCl_4 \cdot 5H_2O$ and 500 mg $Li_4Ti_5O_{12}$ were added into 15 mL ethanol and under ultrasound for 15min, then 0.50 mL ammonium hydroxide (25 wt%) was added and stirred. After isolated by centrifugation and washed

with deinonized water to remove redundant ammonium ions, the white slurry was dried and annealed at 500℃ for 4h. Finally, the powder was mixed with lactose in mass ratio of 5:2 in 25 mL ethanol/water solutions (1/1 by volume ratio) and stirred at 70℃ to vapor the solutions before annealed at 700℃ for 4h under H_2/Ar (volume ratio was 1/19) to obtained final product. For comparing, C-$Li_4Ti_5O_{12}$ was also synthesized by coating lactose on $Li_4Ti_5O_{12}$ and heat treated under N_2 at 550℃.

2.2. Characterizations

For material characterizations, XRD patterns were collected on a Shimadzu-XRD-7000S X-ray diffractometer with Cu-Kα radiation (λ= 1.54056 Å) at a voltage of 40kV and a current of 40 mA. TG was conducted under NETZSCH STA 2500 in a temperature range of 30 to 900 ℃ at air atmospheres with a heated rate of 10 ℃ min^{-1}. Raman spectra were recorded using a Confocal Micro-Raman spectroscopy fitted with a 632.8 nm He-Ne excitation laser. Elemental analysis was operated on vario EL Elemental Analyzer. SEM images were acquired on a S4800 microscope. TEM images were taken on FEI Tecnai G20 microscopes.

2.3 cells assembly and electrochemical testing

To evaluate electrochemical properties, samples (80 wt%), conductive carbon black (10 wt%) and polyvinylidene fluoride (10 wt%) binder were mixed using N-methyl pyrrolidone as solvent for a homogeneous slurry, the slurry was then pasted uniformly onto a copper foil and dried to give the electrodes with loading materials of ~ 2.5 mg cm^{-2}. The 2032 coin cells were assembled in an argon-filled dry glove box using lithium metal foil as the counter electrode. The electrolyte was a 1 M $LiPF_6$ solution in the mixture of ethylene carbonate, dimethyl carbonate and ethylene methyl carbonate (1/1/1 by volume). A polypropylene membrane (Celgard 2400) was used as the separator. CVs were investigated at a scan rate of 0.2 mV s^{-1} by an Autolab PGSTAT 128N. Galvanostatic charge-discharge tests were performed on a LAND battery tester with a cut-off voltage of 0.01 ~ 3.0V. For long cyclamens, the current density in first two cycles was fixed on 20 mA g^{-1}. The capacity was calculated based on the mass of C-Sn/$Li_4Ti_5O_{12}$ and C-$Li_4Ti_5O_{12}$, respectively. All the tests were operated at room temperature.

3. RESULTS AND DISCUSSION

3.1 Physical properties

The crystals structure of C-$Li_4Ti_5O_{12}$ and C-Sn/$Li_4Ti_5O_{12}$ was recorded by XRD and the results were shown in Fig. 1. It can be seen that some diffraction peaks in curve (a) and all the diffraction peaks in curve (b) can be indexed to standard spinel $Li_4Ti_5O_{12}$ (JCPDS No. 49-0207), indicating that there was $Li_4Ti_5O_{12}$ in C-$Li_4Ti_5O_{12}$ and C-Sn/$Li_4Ti_5O_{12}$. For curve (a), besides the standard $Li_4Ti_5O_{12}$ diffraction peaks, all the other diffraction peaks can be unambiguously ascribed to tetragonal Sn

(JCPDS No. 04-0673), suggesting Sn exists in the C-Sn/$Li_4Ti_5O_{12}$. There were no carbon diffraction peaks in XRD patterns may attribute to its low graphitization degree.

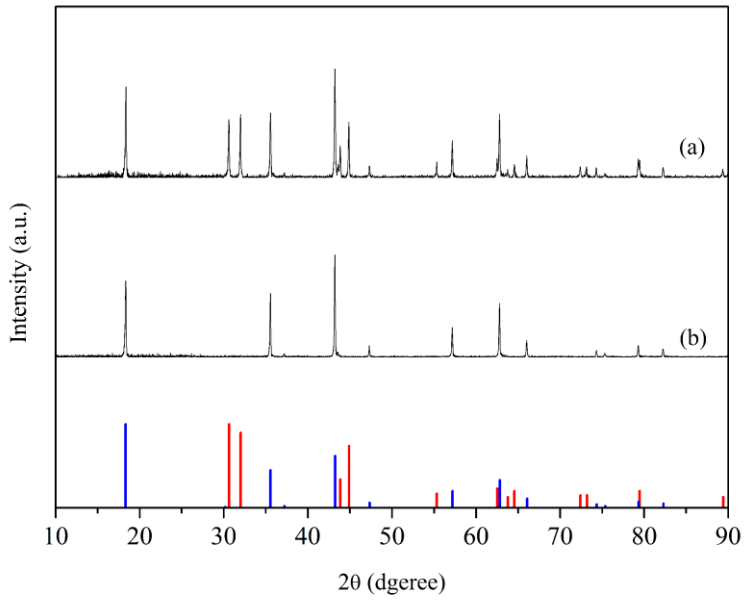

Figure 1. XRD diffraction of C-Sn/$Li_4Ti_5O_{12}$ (a) and C-$Li_4Ti_5O_{12}$ (b). The red and blue bars on bottom are standard Sn and $Li_4Ti_5O_{12}$ diffraction peaks

For understanding elemental content in the samples, C-Sn/$Li_4Ti_5O_{12}$ and C-$Li_4Ti_5O_{12}$ were measured by TG and C-Sn/$Li_4Ti_5O_{12}$ was tested by elemental analysis. TG results were shown in Fig. 2. C-Sn/$Li_4Ti_5O_{12}$ and C-$Li_4Ti_5O_{12}$ exhibited low weight loss under 200 ℃ and continued weight loss between 300℃ and 500 ℃, which was related to the removal of adsorbed water and combustion of carbon, respectively. For C-Sn/$Li_4Ti_5O_{12}$, the weight increased obviously in the temperature ranges of 505 ℃ to 705 ℃, relating to the oxidation of Sn particles. In addition, a temperature plateau from 705 ℃ to 900 ℃ was observed, indicating all the carbon and Sn were oxidized completely. For C-$Li_4Ti_5O_{12}$, there was no weight loss beyond 460℃, indicating all the carbon was oxidized. According to TG of C-Sn/$Li_4Ti_5O_{12}$, there were 93.74 wt% terminal residues that were incombustible $Li_4Ti_5O_{12}$ and new produced SnO_2. Furthermore, the carbon content in C-Sn/$Li_4Ti_5O_{12}$ was 8.63 wt% measured by elemental analysis. The mass content of Sn and $Li_4Ti_5O_{12}$ can be calculated to be 8.78 wt% and 82.59 wt% from TG and elemental analysis data, respectively. Compared with C-Sn/$Li_4Ti_5O_{12}$, the carbon content in C-$Li_4Ti_5O_{12}$ was 6.26 wt%.

Fig. 3 shows SEM and TEM images of the samples. As shown in Fig. 3(a), (b), (d) and (e), the morphology of C-$Li_4Ti_5O_{12}$ and C-Sn/$Li_4Ti_5O_{12}$ inherited the shape of TiO_2 precursor, which was spherical-like particle with average outer diameter of ~ 1μm. In Fig. 3(c), the thickness of carbon layer in the surface of C-$Li_4Ti_5O_{12}$ can be evaluated as ~ 5 nm. Similarly, the thickness of the carbon layer in C-Sn/$Li_4Ti_5O_{12}$ was ~ 10 nm in Fig. 3(e). In Fig. 3(f), the high resolution TEM image shows two types of regular lattices, which corresponds to spinel $Li_4Ti_5O_{12}$ and tetragonal Sn. The results of TEM are

consistent with the results of XRD. More importantly, it is very obvious that Sn particles embed between carbon layer and $Li_4Ti_5O_{12}$ core in Fig. 3(e) and (f).

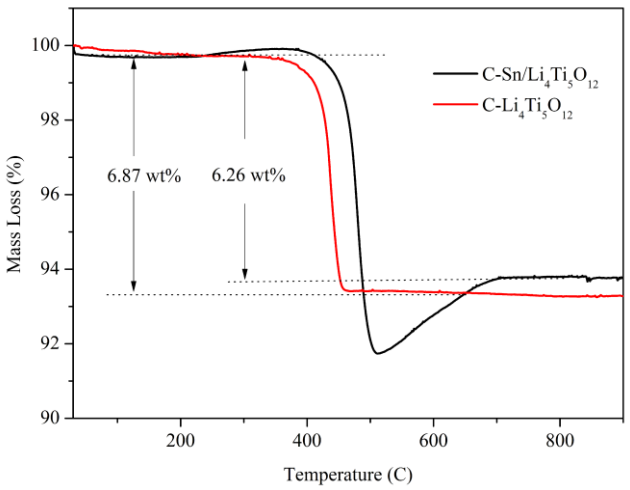

Figure 2. TG curves of C-Sn/$Li_4Ti_5O_{12}$ and C-$Li_4Ti_5O_{12}$

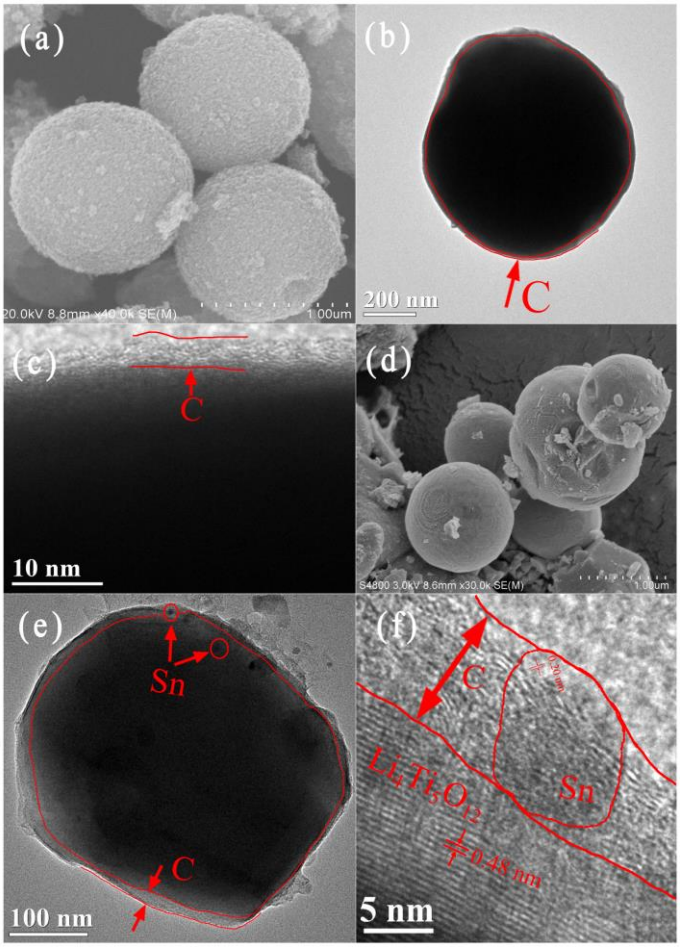

Figure 3. SEM images of TiO_2 spheres (a) and C-Sn/$Li_4Ti_5O_{12}$ (d), TEM images of C-$Li_4Ti_5O_{12}$ (b, c) and C-Sn/$Li_4Ti_5O_{12}$ (e, f)

Besides $Li_4Ti_5O_{12}$ and Sn lattice fringes, some other structure fringes also observed in Fig. 3(f), and the fringes were similar with the carbon layer shown in Fig. 3(c). For understanding carbon ingredients, Fig. 4 shows the Raman spectra of the samples. The intense broad bands at about 1347 and 1586 cm^{-1} were assigned to the disorder (D) and graphene (G) bands of residual carbon in C-Sn/$Li_4Ti_5O_{12}$ composite, respectively. Similarly, the D band and G band of C-$Li_4Ti_5O_{12}$ composite were locate in about 1323 and 1596 cm^{-1}. The G band corresponds to one of the E_{2g} modes, which has been assigned as the sp^2 graphite-like structure, whereas the D band corresponds to one of the A_{1g} modes, which is attributed to the sp^3 type tetrahedral carbon. That is the reason why graphite lattice exists in the coating carbon layer, which is consistent with the Fig. 3(c) and (f). Although there was graphitized carbon in the samples, the graphite diffraction peaks were not reflected in XRD curves [22-24]. Furthermore, the value of I_D/I_G (the peak intensity ratio) can be used to evaluate the content of sp^{3-} and sp^{2-} coordinated carbon in the sample, as well as the degree of disorder carbon layer [25,26]. Theoretically, the low values for the I_D/I_G parameters indicate a high degree of graphitization. The I_D/I_G values of C-$Li_4Ti_5O_{12}$ and C-Sn/$Li_4Ti_5O_{12}$ were calculated as 1.0416 and 0.8874, indicating higher graphitization degree of the carbon layer in C-Sn/$Li_4Ti_5O_{12}$ than that of $Li_4Ti_5O_{12}$, which is caused by high temperature solid state reaction of C-Sn/$Li_4Ti_5O_{12}$ (at 700°C).

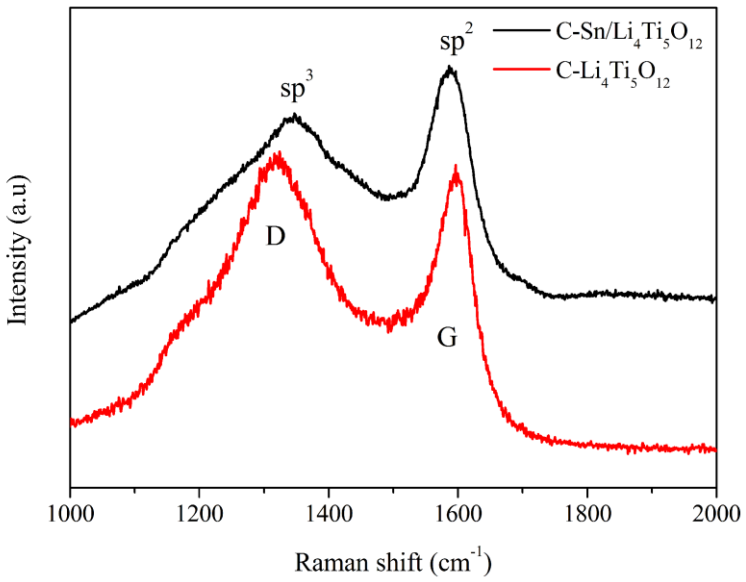

Figure 4. Raman spectra of C-Sn/$Li_4Ti_5O_{12}$ and C-$Li_4Ti_5O_{12}$

3.2 Electrochemical performances

For understanding the lithiation-delithiation reactions, Fig. 5 displays CVs of the samples. It is obvious that C-$Li_4Ti_5O_{12}$ sample show two pairs of redox peaks, the first pair of redox peaks is the characteristics redox peaks of $Li_4Ti_5O_{12}$ (1.68/1.54V), the second pair of redox peaks is attributed to the carbon component in the C-$Li_4Ti_5O_{12}$ composite (below 0.6 V) [27]. However, in Fig. 5(a), besides the typical C-$Li_4Ti_5O_{12}$ redox peaks, there are several redox peaks that are locate at 0.15 ~ 0.8V

(marked as Ⅰ/Ⅰ'; Ⅱ/Ⅱ'; Ⅲ/Ⅲ' and Ⅳ/Ⅳ'). It is proved that those redox peaks are caused by oxidation-reduction behavior of Li_xSn_y (x=1, y=1; x=7, y=2 or 3; x=22, y=5) [28-30].

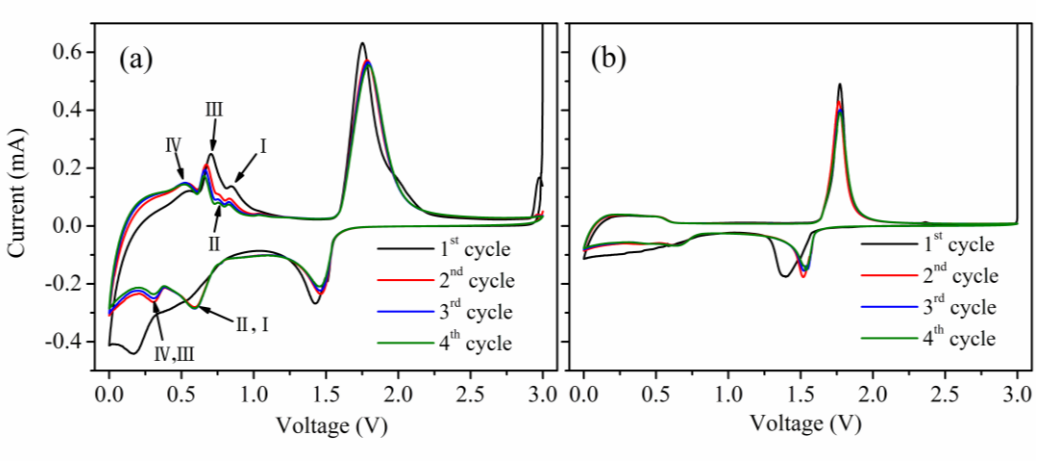

Figure 5. CVs of C-Sn/$Li_4Ti_5O_{12}$ (a) and C-$Li_4Ti_5O_{12}$ (b)

In order to evaluate cycle performance of the samples, the cells were charged and discharged in a series of stages with different current densities from 50 mA g^{-1} to 500 mA g^{-1}. Fig. 6 shows the variation of discharge capacity in the cycle process. In each stage, both C-Sn/$Li_4Ti_5O_{12}$ and C-$Li_4Ti_5O_{12}$ kept stable discharge capacity even at 500 mA g^{-1} though the discharge capacity decreased gradually with the increasing of current density. Significantly, C-Sn/$Li_4Ti_5O_{12}$ showed higher discharge capacity than C-$Li_4Ti_5O_{12}$ in every cycle stage due to the existence of Sn particles. For C-Sn/$Li_4Ti_5O_{12}$ and C-$Li_4Ti_5O_{12}$, the discharge capacity recovered when the current switched to initial 50 mA g^{-1}, indicating good reversibility of as-prepared samples.

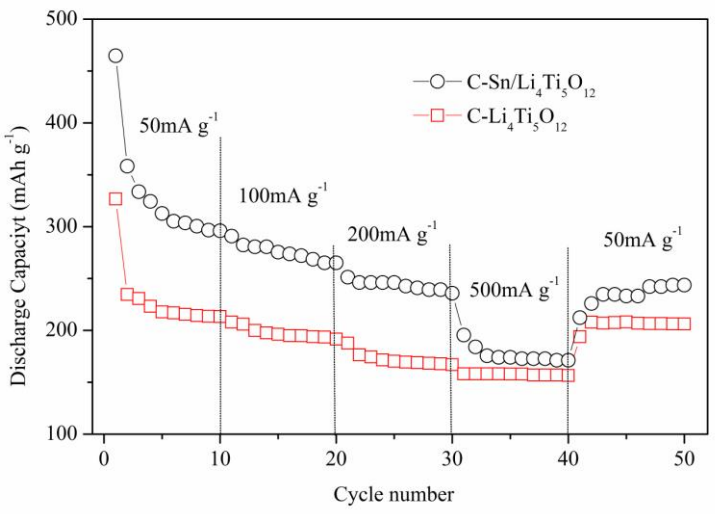

Figure 6. Stage charge-discharge performance of the samples from 50 mA g^{-1} to 500 mA g^{-1}

To further understand the electrochemical performances, the cycle curves of C-Sn/$Li_4Ti_5O_{12}$ and C-$Li_4Ti_5O_{12}$ at 200 mA g^{-1} were shown in Fig. 7. The results indicate that a high stable discharge

capacity of ~ 250 mAh g $^{-1}$ for C-Sn/$Li_4Ti_5O_{12}$ was obtained after first few cycles activated, while C-$Li_4Ti_5O_{12}$ was ~ 215 mAh g $^{-1}$ at the same conditions. After the electrodes become stable, the coulombic efficiencies of C-Sn/$Li_4Ti_5O_{12}$ and C-$Li_4Ti_5O_{12}$ were close to 100%, exhibiting high reversibility of as-prepared samples. The stable discharge capacity of C-Sn/$Li_4Ti_5O_{12}$ was improved by ~ 16.3% than that of C-$Li_4Ti_5O_{12}$, confirming that a certain amount of Sn in C-Sn/$Li_4Ti_5O_{12}$ can increase its discharge capacity significantly. Some similar works were studied such as ref. [13] and ref. [14]. In ref. [13], Sivashanmugam et al. prepared novel $Li_4Ti_5O_{12}$/Sn nano-composite via high-energy mechanical milling of $Li_4Ti_5O_{12}$ and nano-Sn. The composites of 10 wt% Sn/90 wt% $Li_4Ti_5O_{12}$ and 30 wt% Sn/70 wt% $Li_4Ti_5O_{12}$ delivered stable capacity of 200 mAh g^{-1} and 300 mAh g^{-1} after 30 cycles activated, respectively, but the cycled current was only 0.1 mA cm^{-2} (C/50). In ref. 14, Cai et al. synthesized $Li_4Ti_5O_{12}$/Sn composite anode with the weight ratio 9:1 of $Li_4Ti_5O_{12}$ to Sn. The $Li_4Ti_5O_{12}$/Sn composite maintained 224 mAh g^{-1} after 50 cycles at 100 mA g^{-1}. It is obvious that its cycle performance is much worse than that of C-Sn/$Li_4Ti_5O_{12}$ in this work, which was due to no carbon existence in the $Li_4Ti_5O_{12}$/Sn composite. Compared with previous works, the improved electrochemical performances of C-Sn/$Li_4Ti_5O_{12}$ may be attributed to two reasons. One is that embedded Sn can provide a high discharge capacity for the electrode. The other is that the highly encapsulated conductive carbon coating layer can provide an excellent conductive web for electrons, more importantly, alleviate the volume change of embedded Sn during cycling.

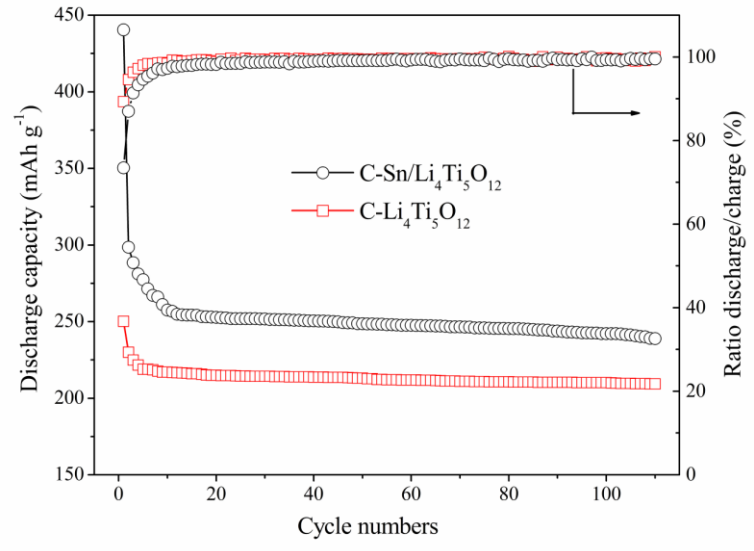

Figure 7. Cycle performance of the samples at 200 mA g^{-1}

The charge-discharge behavior of C-Sn/$Li_4Ti_5O_{12}$ and C-$Li_4Ti_5O_{12}$ for the 1st, 10th and 100th cycles was recorded as Fig. 8 at the same time when cycled at 200 mA g^{-1}. As shown in the figure, first charge-discharge curves were different between C-Sn/$Li_4Ti_5O_{12}$ and C-$Li_4Ti_5O_{12}$. The capacity of C-Sn/$Li_4Ti_5O_{12}$ was much higher than C-$Li_4Ti_5O_{12}$, and the plateau of Sn in charge-discharge curves can be seen clearly. The differences exhibited Sn existed in the C-Sn/$Li_4Ti_5O_{12}$ composite and played an

important role in Li^+ reaction, which was consistent with the results of CVs. However, the charge-discharge curves were similar between 10^{th} and 100^{th} in the C-Sn/$Li_4Ti_5O_{12}$ and C-$Li_4Ti_5O_{12}$, suggesting that the charged-discharge plateaus of Sn and $Li_4Ti_5O_{12}$ were overlapped into a rather smooth plateau. The overlapped plateau should be own to the neighboring of the broad $Li_4Ti_5O_{12}$ redox peaks blow 0.6V and the Sn redox peaks at 0.15 ~ 0.8V, which was detected by CVs. Furthermore, the minute differences between 10^{th} and 100^{th} indicated stable cycle performance of C-Sn/$Li_4Ti_5O_{12}$ and C-$Li_4Ti_5O_{12}$, which corresponded to the results of Fig. 7.

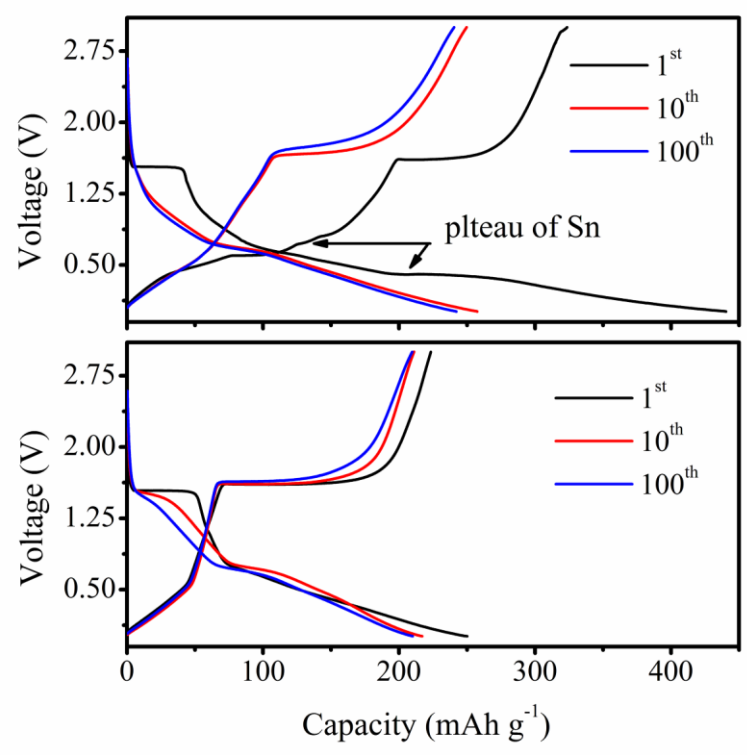

Figure 8. Charge-discharge behavior of C-Sn/$Li_4Ti_5O_{12}$ (a) and C-$Li_4Ti_5O_{12}$ (b) for the 1^{st}, 10^{th} and 100^{th} cycles

4. CONCLUSIONS

An efficient approach for the preparation of Sn embedded $Li_4Ti_5O_{12}$/C composite (C-Sn/$Li_4Ti_5O_{12}$) with reasonable electrochemical properties has been developed. In this study, an average particle size of C-Sn/$Li_4Ti_5O_{12}$ was about 1um. Sn particles act as higher specific capacity material, carbon-coated layer acts as electronic conductor and volume buffer layer to hind the volume change of Sn during cycling. The Sn and carbon-coated layer have a positive effect on the electrochemical performance of $Li_4Ti_5O_{12}$ anode. At 200 mAh g^{-1}, the discharge capacity of as-prepared C-Sn/$Li_4Ti_5O_{12}$ was stable after first few cycles and reached ~ 242 mAh g^{-1} after 100 cycles, which was improved by ~ 16.3% than that of C-$Li_4Ti_5O_{12}$. These results indicate a high capacity anode material

can be fabricated using Sn as a doping material and carbon as a coating layer, which is proved as an effective way to improve the discharge capacity of anode.

ACKNOWLEDGMENTS
This work was supported by the National Natural Science Foundation of China (No. 21206203), Program for Chongqing Science & Technology Innovation Talents (cstc2013kjrc-qnrc50006) and the Scientific Research Innovation Team of Chongqing University of Technology (No. cqut2015srim).

References

1. J. Liu, W. Liu, Y. L. Wang, S. M. Ji, J. B. Wang and Y. C. Zhou, *RSC Adv*., 2 (2012) 10470.
2. C. Wang, S. Wang, Y. B. He, L. Tang, C. Han, C. Yang, M. Wagemaker, B. H. Li, Q. H. Yang, J. K. Kim and F. U. Kang, *Chem. Mater*., 7 (2015) 5647.
3. X. Lu, L. Gu, Y. S. Hu, H. C. Chiu, H. Li, G. P. Demopoulos and L. Q. Chen, *J. Am. Chem. Soc.*,137 (2015) 1581.
4. J. Liu, K. P. Song, P. A. van Aken, J. Maier and Y. Yu, *Nano Lett*., 14 (2014) 2597.
5. E. Pohjalainen, T. Rauhala, M. Valkeapää, J. Kallioinen and T. Kallio, *J. Phys. Chem*. C, 119 (2015) 277.
6. R. Raccichini, A. Varzi, S. Passerini and B. Scrosati, *Nat. Mater*., 14 (2015) 271.
7. A. Nugroho, S. J. Kim, K. Y. Chung, B. W. Cho, Y. W. Lee and J. Kim, *Electrochem. Commun*., 13 (2011) 650.
8. T. F. Yi, Y. Xie, Y. R. Zhu, R. S. Zhu and H. Shen, *J. Power. Sources*, 222 (2013) 448.
9. Z. Z. Yu, G. S. Zhu, H. R. Xu and A. Yu, *Energy Technol*., 2 (2014) 767.
10. K. M. Yang, Y. C. Kang, S. M. Jeong, Y. J. Choi and Y. S. Kim, *Int. J. Electrochem*., 8 (2013) 11972.
11. S. Y. Han, I. Y. Kim, S. H. Lee and S. J. Hwang, *Electrochim. Acta*, 74 (2012) 59.
12. L. Z. Xiong, Z. Q. He, Z. L.Yin and Q. Y. Chen, *Trans. Nonferrous Met. Soc. China*, 20 (2010) s267.
13. A. Sivashanmugam, S. Gopukumar, R. Thirunakaran, C. Nithya and S. Prema, *Mater. Res. Bull.*, 46 (2011) 492.
14. R. Cai, X. Yu, X. Q. Liu and Z. P. Shao, *J. Power. Sources*, 195 (2010) 8244.
15. M. Uysal, T. Cetinkay, A. Alp and H. Akbulut, *J. Alloy. Compd*., 645 (2015) 235.
16. J. S. Cho and Y. C. Kang, *Small*, 11 (2015) 4673.
17. P. C. Lian, J. Y. Wang, D. Y. Cai, G. X. Liu, Y. Y. Wang and H. H. Wang, *J. Alloy. Compd*., 604 (2014) 188.
18. Y. Zhong, X. F. Li, Y. Zhang, R. Y. Li, M. Cai and X. L. Sun, *Appl. Surf. Sci*., 332 (2015) 192.
19. S. L. Li, C. Chen, K. Fu, L. G. Xue, C. X. Zhao, S. Zhang, Y. Hu, L. Zhou and X. W. Zhang, *Solid State Ionics*, 254 (2014) 17.
20. C. Y. Cui, X. G. Liu, N. D. Wu and Y. P. Sun, *Mater. Lett*., 143 (2015) 35.
21. L. S. Zhong, J. S. Hu, L. J. Wan and W. G. Song, *Chem. Commun*., 10 (2008) 1184.
22. L. F. Shen, X. G.Zhang, E. Uchaker, C. Z. Yuan and G. Z. Cao, *Adv. Energy Mater*., 2 (2012) 691.
23. Z. Q. Zhu, F. Y. Cheng and J. Chen, *J. Mater. Chem*. A, 1 (2013) 9484.
24. Z. M. Liu, N. Q. Zhang and K. N. Sun, *J. Mater. Chem*., 22 (2012) 11688.
25. L. Wen, Z. Y. Wu, H. Z. Luo, R. S. Song and F. Li, *J. Electrochem. Soc*., 162 (2015) A3038.
26. X. B. Hu, Z. Y. Lin, K. R. Yang, Y. J. Huai and Z. H. Deng, *Electrochimica Acta*, 56 (2011) 5046.
27. W. M. Zhang, J. S. Hu, Y. G. Guo, S. F. Zheng, L. S. Zhong, W. G. Song and L. J. Wan, *Adv. Mater*., 20 (2008) 1160.
28. G. Wang, Y. Q. Ma, Z. Y. Liu and J. N. Wu, *Electrochim. Acta*, 65 (2012) 275.

29. Z. X. Chen, Y. L. Cao, J. F. Qian, X. P. Ai and H. X. Yang, *J. Mater. Chem.*, 20 (2010) 7266.
30. L. M. Sun, X. H. Wang, R. A. Susantyoko and Q. Zhang, *Carbon*, 82 (2015) 282.